University of Wollongong

Research Online

Australian Institute for Innovative Materials - Papers

Australian Institute for Innovative Materials

1-1-2016

Functional 3D neural mini-tissues from printed gel-based bioink and human neural stem cells

Qi Gu
University of Wollongong, qg863@uowmail.edu.au

Eva Tomaskovic-Crook
University of Wollongong, evatc@uow.edu.au

Rodrigo Lozano
University of Wollongong, rl137@uowmail.edu.au

Yu Chen
University of Wollongong, yc456@uowmail.edu.au

Robert M. I Kapsa
University of Wollongong, robk@uow.edu.au

See next page for additional authors

Follow this and additional works at: https://ro.uow.edu.au/aiimpapers

🔴 Part of the Engineering Commons, and the Physical Sciences and Mathematics Commons

Functional 3D neural mini-tissues from printed gel-based bioink and human neural stem cells

Abstract

Direct-write printing of stem cells within biomaterials presents an opportunity to engineer tissue for in vitro modeling and regenerative medicine. Here, a first example of constructing neural tissue by printing human neural stem cells that are differentiated in situ to functional neurons and supporting neuroglia is reported. The supporting biomaterial incorporates a novel clinically relevant polysaccharide-based bioink comprising alginate, carboxymethyl-chitosan, and agarose. The printed bioink rapidly gels by stable cross-linking to form a porous 3D scaffold encapsulating stem cells for in situ expansion and differentiation. Differentiated neurons form synaptic contacts, establish networks, are spontaneously active, show a bicuculline-induced increased calcium response, and are predominantly gamma-aminobutyric acid expressing. The 3D tissues will facilitate investigation of human neural development, function, and disease, and may be adaptable for engineering other 3D tissues from different stem cell types.

Disciplines

Engineering | Physical Sciences and Mathematics

Publication Details

Authors

Qi Gu, Eva Tomaskovic-Crook, Rodrigo Lozano, Yu Chen, Robert M. I Kapsa, Qi Zhou, Gordon G. Wallace, and Jeremy Micah Crook

Title: Functional 3D Neural Mini-Tissues From Printed Gel-Based Bioink And Human Neural Stem Cells

Author(s), and Corresponding Author(s)* Qi Gu, Eva Tomaskovic-Crook, Rodrigo Lozano, Yu Chen, Robert M. Kapsa, Qi Zhou, Gordon G. Wallace*, and Jeremy M. Crook*

Dr. Q. Gu, Dr. E Tomaskovic-Crook, Mr R Lozano, Mr Y Chen, Prof. R. M. Kapsa, Prof. G. G. Wallace, Assoc. Prof. J. M. Crook
ARC Centre of Excellence for Electromaterials Science, Intelligent Polymer Research Institute, AIIM Facility, Innovation Campus, University of Wollongong, Squires Way, Fairy Meadow, New South Wales 2519, Australia
E-mail: jcrook@uow.edu.au or gwallace@uow.edu.au
Dr. E Tomaskovic-Crook, Assoc. Prof. J. M. Crook
Illawarra Health and Medical Research Institute, University of Wollongong, Wollongong, New South Wales 2522, Australia
Dr. Q. Gu, Prof. Q Zhou
State Key Laboratory of Stem Cell and Reproductive Biology, Institute of Zoology, Chinese Academy of Sciences, Beijing, 100101, P.R. China
Assoc. Prof. J. M. Crook
Department of Surgery, St Vincent's Hospital, The University of Melbourne, Fitzroy, Victoria 3065, Australia
Prof. R. M. Kapsa
Department of Medicine, St Vincent's Hospital, The University of Melbourne, Fitzroy, Victoria 3065, Australia

Direct-write printing of stem cells within biomaterials presents an opportunity to engineer tissue for *in vitro* modelling and regenerative medicine. Here we report a first example of constructing neural tissue by printing human neural stem cells (hNSCs) that are differentiated *in situ* to functional neurons and supporting neuroglia. The supporting biomaterial incorporates a novel clinically relevant polysaccharide-based bioink comprising alginate (Al), carboxymethyl-chitosan (CMC) and agarose (Ag). The printed bioink rapidly gels by stable crosslinking to form a porous 3D scaffold encapsulating stem cells for *in situ* expansion and differentiation. Differentiated neurons are spontaneously active, show a bicuculline-induced increased calcium response, and are predominantly gamma-aminobutyric acid (GABA) expressing. The 3D tissues will facilitate investigation of human neural development, function and disease, and may be adaptable for engineering other 3D tissues from different stem cell types.

1. Introduction

3D bioprinting to generate functional tissues has been made possible by recent advances in

printing technology, materials science and stem cell science. Also known as additive

biofabrication, 3D bioprinting has provided a paradigm shift in *in vitro* tissue engineering, as a potential remedy to limited supply of functional tissues for modelling development and disease, and transplantation therapy[1]. Bioprinting enables specification of extracellular features and cell organisation for increased control of 3D tissue fabrication. Compared to traditional 2D methods of cell culture in monolayers, 3D printed cultures better recapitulate the natural cell environment and cell-cell interaction for more authentic, reliable and clinically relevant tissue generation. Key features of a printed construct include porosity for diffusion of oxygen and nutrients, and correct mechanochemistry of component biomaterials to promote cell adhesion, survival, networking and function[2].

Strategies for additive tissue fabrication include printing of biomaterial scaffolds that are seeded with cells following printing[3], or concomitant (co-) printing of biomaterials and cells resulting in encapsulated cell constructs[3-9]. The strategy of co-printing offers many advantages including immediate integration of cells with printed biomaterials, more rapid production of a construct, and more authentic simulation of the *in vivo* tissue environment whereby cells are completely surrounded by and in direct contact with extracellular components and other cells. These features serve to provide a simpler, more automated and defined approach to biomaterial-cell interfacing for reproducible, robust and germane construct development.

Here we report a well-defined and reproducible method for making a novel 3D neural mini-tissue construct (nMTC) by microextrusion bioprinting frontal cortical hNSCs with a supporting bioink followed by *in situ* differentiation to functional neurons and supporting neuroglia. The bioink comprises polysaccharides Al, CMC and Ag, which form a gel by chemical crosslinking following extrusion with hNSC encapsulation. Al and Ag provide structural support for the construct, with Al enabling gelation in the presence of cations after printing and Ag conferring suitable bioink viscosity during printing prior to gelation. CMC is a water soluble derivative of chitosan and conducive to cell survival within the construct.

2

hNSCs can be maintained as self-renewing cells following printing, continuing to proliferate *in situ* for approximately 10 days. Differentiation of hNSCs principally results in GABAergic neurons, together with glial cells expressing astrocyte and oligodendrocyte lineage markers. Importantly, neurons are spontaneously active and show a bicuculline-induced increased calcium response, indicative of the presence of receptors for GABA and therefore GABA responsive neurons, and consistent with the occurrence of aforementioned GABAergic neurons. Finally, the method will enable interrogation of neural development, function and disease and may be adaptable for generating other neuronal and non-neuronal MTCs *in vitro*. Moreover, the MTCs have the potential to be used to develop larger macro-tissue constructs by either "rational design", "autonomous assembly" or both[1].

2. Results and Discussion

2.1. Bioprinting hNSC-Laden Al-CMC-Ag Gel Constructs

To generate hNSC-laden gel constructs we developed a printable bioink of 5% weight per volume (w/v) Al, 5% w/v CMC and 1.5% w/v Ag (**Figure 1**A-C; Video S1, Supporting Information). Inks comprising lower (0.5% w/v) or higher (2.5% w/v) Ag concentrations were associated with lower and higher viscosities respectively resulting in poorly defined scaffold structures (**Figure 1**D). Printability of the optimal bioink was supported by its uniform consistency, with minimal fluctuations in extrusion force (around 8.5 N) required for printing and indicative of homogeneity within the solution (**Figure 1**E). Homogeneity was also reflected by uniform hNSC distribution and viability throughout the construct immediately following printing (**Figure 1**C). As expected, lower viscosity water control showed a similarly constant but lower magnitude (around 2 N) extrusion force profile (**Figure 1**E).

Ink gelation following ionic-crosslinking resulted in an initial compression modulus (E_{Comp}) of around 7.5 kilopascals (kPa), with an indentation modulus (E_{Ind}) of around 4.75

kPa. While subsequent temporal analysis of E_{Ind} indicated decreasing stiffness of the gel, the rate of change diminished towards stabilising at around 0.8 kPa by day 10 (**Figure 1**F).

Gel porosity was examined in the absence of cells by low vacuum scanning electron microscopy (SEM), with freeze-fracturing for internal analysis. Surface scanning of gels comprising different concentrations of CMC indicated variable porosity, with 5% and 3.5% w/v CMC associated with a highly and sparsely porous surface respectively, and 2% or less w/v CMC gels associated with negligible to no pores (**Figure 2**A). SEM of the gel interior revealed an assembly of polyhedral pores throughout regardless of CMC content, although a range of pore diameters were observed (**Figure 2**B). Therefore, gels with 5% and 3.5 % w/v CMC comprised a network of larger and smaller sized pores, with the smaller pores often connecting the larger pores. In contrast, gels with 2% or less w/v CMC principally comprised larger pores, with relatively few small pores.

Intrinsic gel permeability was studied by measuring the uptake of bovine serum albumin (BSA) by 5% and 3.5% w/v CMC gels and applying a non-steady state diffusion model[10]. For both gels, BSA uptake reached equilibrium by 8 h (**Figure 2**C), also shown by finite element modelling (COMSOL; **Figure 2**D). The diffusion coefficients were 6.56 x 10^{-7} and 5.56 x 10^{-7} for 5% and 3.5% w/v CMC gels respectively. Further studies of 5% w/v CMC gels using confocal microscopy image-based analysis confirmed the rate of uptake and diffusion of BSA throughout the gel (**Figure 2**E; Video S2 and Figure S1, Supporting Information).

2.2. Characterisation of Encapsulated hNSCs

Initial studies of hNSC survival and proliferation within the printed gel construct showed CMC content of the gel influenced hNSC viability, with preferred 5% w/v associated with greater cell loading (indicated by area measures of individual cells and cell aggregates)

4

compared to lower concentrations (F (3, 580) = 22.77, $P < 0.0001$). Furthermore, there was a significant difference in the effect of CMC content with increasing days of culture (F (11, 580) = 13.82, $P < 0.0001$). Following 9 days culture of 5% w/v CMC-gel constructs, Bonferroni *post hoc* analysis revealed cell support to be significantly greater than gel constructs with lower CMC content at any time during culture ($P < 0.0001$; **Figure 3**A,B), while support by gel constructs with 5% and 3.5% w/v CMC content at day 5 culture was greater than Al-Ag alone (ie. no CMC) at day 9 of culture ($P < 0.01$ and $P < 0.05$ respectively; **Figure 3**A,B). Although cell loading of 5% w/v CMC gel increased for the duration of culture (indicative of hNSC proliferation), loading decreased from the time of printing for gels with no or 2% w/v CMC, while 3.5% w/v CMC gel supported an initial increase up to day 5 with subsequent reduced cell loading apparent by day 9 post-printing (**Figure 3**A,B). Area measurements of viable cells and aggregates in the gels comprised a wide range of values (manifest as large standard deviations, Levene's Test (Absolute deviations), F (11, 580) = 7.59, $P < 0.0001$), indicative of a large range of hNSC aggregate sizes (**Figure 3**B). Importantly, the population variances were not significantly different according to Levene's Test (Squared deviations; $P = 0.68$ (F (11, 580) = 0.75)), satisfying homogeneity of variance testing for statistical analysis by ANOVA.

Further growth profiling of viable and dead cells over time within optimal 5% w/v CMC gel demonstrated relatively high (around 25%) cell death immediately after printing (day 0), with the proportion of dead hNSCs subsequently decreasing (F (7, 30) = 14.10, $P < 0.0001$) to being statistically significant on day 4 post-printing ($P < 0.001$), continuing to around 8% by day 6 (**Figure 3**C). Live cell analysis supported cell proliferation (F (9, 20) = 146.62, $P < 0.0001$), reaching significantly different on day 5 compared to day 1 after printing ($P < 0.0001$), before peaking at day 11 (**Figure 3**D). Confocal microscopy revealed persistent homogenous live cell distribution throughout the constructs, with hNSCs visible as single

cells on day 1 following printing, and aggregates of cells increasingly apparent thereafter (day 3 – day 11) (**Figure 3**E; Figure S2, Supporting Information).

Immunophenotyping at 3 weeks post-printing demonstrated hNSCs expressed undifferentiated cell markers SOX2 (**Figure 4**A,C), vimentin (**Figure 4**A,D) and nestin (**Figure 4**B), as well as the nuclear proliferation marker KI67 (**Figure 4**B). Negligible levels of the differentiation and neuronal-specific cytoskeleton protein TUJ1 (**Figure 4**C), astrocyte marker glial fibrillary acidic protein (GFAP) and oligodendrocyte lineage transcription factor 2 (OLIGO2) were expressed (**Figure 4**D).

2.3. Characterisation of *In Situ* Differentiated hNSCs

Based on hNSC growth profiling we opted to explore *in situ* differentiation by inducing hNSCs to functional neurons and neuroglia 10 days post-printing. Immunophenotyping 2 weeks after initiating differentiation revealed neurons that expressed TUJ1 (**Figure 5**A; Video S3, Supporting Information), GABAergic markers GABA and glutamic acid decarboxylase (GAD) (**Figure 5**B), with concomitant low SOX2 expression (**Figure 5**A). OLIGO2 and GFAP expression were mutually exclusive (**Figure 5**C), and presynaptic vesicle glycoprotein synaptophysin was apparent as small puncta often adjacent to cell bodies (**Figure 5**D). In addition, immunolabelling of TUJ1 3 weeks after differentiation confirmed persistent cell viability within constructs, with neuronal cell clusters interconnected by neurites (**Figure 5**E).

Gene expression analysis by reverse-transcription quantitative PCR (RT-qPCR) corroborated immunophenotyping by showing upregulation of pan-neuronal and neuroglial markers along with neuronal sub-type specific markers under differentiation conditions (**Figure 5**F). RT-qPCR also included comparison between 3D and conventional planar hNSC culture and differentiation, with 3D differentiation predominantly associated with higher transcript levels for neuronal and neuroglial markers compared to 2D differentiation (**Figure**

5F). Specifically, *in situ* 3D differentiation induced a higher expression of *TUJ1* (F (3, 4) = 1380.21), *GFAP* (F (3, 4) = 55171.42), *OLIGO2* (F (3, 4) = 1667.92) and *synaptophysin* (F (3, 4) = 315.75) mRNA compared to undifferentiated 3D hNSC constructs, and conventional 2D culture and differentiation (**Figure 5**F). Interestingly, *GFAP* expression was markedly increased. Also, 3D gel-based differentiation accelerated upregulation of GABAergic neuronal marker *GABA* (F (3, 4) = 1239.48), and to a lesser extent other GABAergic markers *NKX2.1* (F (3, 4) = 69.52) and *MYST* (F (3, 4) = 2172.40), as well as transcripts relevant to other neuronal subtypes included, *vesicular glutamate transporter* (*VGLT*; F (3, 4) = 769.13), *serotonin transporter* (*SRT*; F (3, 4) = 315.75) and serotonin neuronal maker *PET1* (F (3, 4) = 11.66) (**Figure 5**F).

We next investigated functional maturation of *in situ* differentiated hNSCs by measuring spontaneous and bicuculline-induced calcium response of neurons. Neurons displayed spontaneous calcium spikes (**Figure 6**A; Video S4, Supporting Information), and recurrent bursting activity was induced through disinhibition of cells by application of bicuculline, a GABA(A) receptor antagonist (**Figure 6**B; Video S5, Supporting Information).

A final assessment of neurons within the 3D construct was made by SEM, revealing cells with rounded soma and extensive neurite outgrowth (**Figure 6**C).

3. Conclusion

3D extrusion bioprinting offers a versatile platform for fabricating human cell-based tissue constructs from novel clinically-relevant biomaterial-cell combinations. To date, several examples of cell printing have been described and include human dermal fibroblasts and umbilical vein endothelial cells (HUVECs)[3], hepatocarcinoma cells (HepG2)[4], adipose stem cells[5, 6], and mesenchymal stromal cells[6]. Non-human cell printing has included murine

embryonic stem cells for *in situ* embryoid body formation[7], and primary murine cortical neurons and myoblasts[8, 9].

Here we describe the first example of direct-write printing of hNSC-laden bioink to engineer a novel functional 3D nMTC. Co-printing of cells with the bioink provides an efficient, defined and simple approach to biomaterial-cell interfacing, with post-printing gelation resulting in cell encapsulation for *in situ* hNSC expansion and differentiation. The 3D tissues generated are amenable to characterisation for studying neural development and function, including understanding how microenvironmental features affect cell and tissue phenotypes, and have the potential to be adapted to other stem cell types for generating neuronal and non-neuronal tissues *in vitro*. Importantly, the bioink comprises widely available, inexpensive and well characterised components Al, CMC and Ag that have been optimally combined to form a printable, clinically-compatible gel. The consistency of the bioink solution underpins its reliability for printing constructs anew and constructs that are homogenous for uniform cell supportability. This is reflected by demonstrated homogenous hNSC distribution and viability throughout the construct following printing. Studies of modulus after gelation quantitate the mechanical stiffness and therefore construct integrity necessary for post-printing maintenance and handling, and cell support. The stiffness of our gel is in the range of human brain tissue, with previous reports of *in vivo* stiffness ranging from 0.5 - 14 kPa[11-14]. While temporal studies of indentation modulus suggest an initial rapid decrease in stiffness, the diminishing rate of reduction combined with hNSC survival, proliferation and differentiation support enduring biocompatibility with lower gel moduli.

The mechanical properties of a gel, including the modulus and porosity of the matrix environment, affect cell behaviour such as proliferation and differentiation[15]. Although Al was initially chosen as the basis of the gel due to its recognised stability as a 3D structure, low toxicity, and cytocompatible gelation, CMC sustained hNSC survival ostensibly by influencing gel porosity and permeability, while Ag provided requisite bioink viscosity for

8

optimal Ag-CMC printing. Other known properties conceivably beneficial to our approach include high moisture retention of CMC, and antimicrobial and low inflammatory responses of both Al and CMC, all features conducive to cell support and survival[16, 17]. Moreover, as a derivative of chitosan, CMC is deemed to have low to absent toxicity, no mutagenic effects, affects cellular expression of growth factors, and promotes cell adhesion, migration and proliferation[2, 18].

Characterisation of cells within our system support hNSC self-renewal for several weeks following printing and therefore the ability to scale-up hNSC number *in situ* prior to differentiation. Importantly, hNSCs can be induced to functional neurons and supporting neuroglia, with gene expression analysis by RT-qPCR indicating differentiation of stem cells in the 3D constructs may be advantageous compared to conventional 2D platforms for accelerated neuronal, neuroglial and synapse formation. Interestingly, the highly expressed glial marker GFAP is consistent with its key role in central nervous system (CNS) processes including astrocyte-neuron interactions as well as cell-cell communication, with the latter extending to astrocyte mediated synapse formation and function[19-21]. The system may also bias neuronal differentiation to GABAergic lineage, making it attractive for inhibitory neuronal and tissue modelling. Notwithstanding, the occurrence of other neuronal subtypes including glutamatergic and serotonergic, indicate the potential for more expansive modelling, with the possibility of enriching subtype neuronal expression through, for example, cytokine supplementation[22].

Finally, calcium imaging of functioning neurons within the 3D construct together with SEM imaging of neurons and neurites with complex 3D morphologies demonstrate platform utility for modelling human neural cell form and activity, and fabricating functional 3D human neural tissue. As such, the platform is amenable to translational drug-screening *in vitro*, studying human neurodevelopment and disease, and possibly neural tissue engineering for CNS tissue replacement.

4. Experimental Section

hNSC Culture and Differentiation: Working stocks of hNSCs (Millipore: SCC007) were maintained by standard 2D culture, seeding at a density of 2-3 x 10^6 cells into low-attachment 6-well plates (Corning) containing NeuroCult™ NS-A Basal Medium (Human; Stem Cell Technologies) supplemented with heparin (2 µg/ml; Sigma), epidermal growth factor (EGF, 20 ng/ml; Peprotech) and basic fibroblast growth factor (bFGF, 20 ng/ml; Peprotech). hNSCs were passaged for subculture every 5-7 days by digesting in TrypLE (1-2 ml; Gibco BRL) for 3 min at 37°C. Digested cultures were triturated to single cells, and plated at a density of $5x10^4$ cells/ml using low-attachment 6-well plates (Corning).

hNSCs were differentiated by digesting cultures as above and plating $5x10^4$ cells/cm^2 onto 6-well plates (Greiner Bio-One) coated with laminin (20 µg/ml; Life Technologies) containing 2 parts DMEM F-12 : 1 part Neurobasal supplemented with 2% StemPro (Life Technologies), 0.5% N2 (Gibco) and brain-derived neurotrophic factor (BDNF; 50 ng/ml; Peprotech) up to 7 days. A half-volume medium change was performed every 2-3 days.

For 3D hNSC culture and differentiation, the same media employed for 2D culture and differentiation were used, however, washing of printed constructs was performed immediately after printing and gelation (see Bioprinting below). Washing was performed by rinsing constructs for 1 min three times in 37°C culture medium followed by two 10 min washes and 1 h incubation in media before ongoing culture with penicillin (100 U/ml) and streptomycin (100 µg/ml; Life Technologies) under 5% CO_2 at 37°C.

Cells used in this study are approved for use by the University of Wollongong's Human Research Ethics Committee (HE14/049), and regularly tested and maintained mycoplasma free.

Bioink Preparation: Different concentrations of agarose (Ag; Biochemicalsc.Com.Au) solution (including 0.5, 1.5 or 2.5% w/v) were prepared in phosphate-buffered saline (PBS; pH7.4) by heating in a microwave oven, with agitation every 5 sec. Alginate (Al; MW ~50,000 Da, M/G ratio of 1.67, viscosity of 100–300 cP for 2 w/w solution, 25°C; Sigma-Aldrich Pty Ltd) was added to give 5% w/v and stirred at 60 °C for 30 min. Finally, carboxymethyl-chitosan (CMC; Shanghai Dibai Chemical Pty Ltd) was added to give 2, 3.5 or 5% w/v and stirred at 60 °C for a 1 h. The final solutions were subsequently cooled to RT, ready for combining with hNSCs and direct-write printing.

Bioprinting: Samples were extrusion printed into a cubic construct (10mm x 10mm x 10mm) using a 3D-Bioplotter® System (EnvisionTEC GmbH; Video S1, Supporting Information). hNSC-laden bioink samples comprised 5×10^6 cells suspended in bioink (0.5 ml). Samples were loaded into a 55CC barrel (Nordson Australia Pty Ltd), centrifuged at 1000rpm, 15 °C for 1 min to remove air bubbles, placed in the printing magazine, and fitted with a 200 µm printing nozzle (Nordson Australia Pty Ltd). Blender™ open source software was employed to design the scaffold and translated into numerical code for printing onto autoclaved glass slides at 15 °C. The applied pressure for optimal bioink was 1.5-2.0 bar. Following printing, scaffolds were immersed in 2% w/v calcium chloride for 10 min for crosslinking[23].

Bioink Consistency Measurement: Bioink consistency was measured using previously described method[9, 24]. Briefly, variations in extrusion force were measured during sample deposition in real-time. Samples were loaded into a syringe with the plunger coupled to the upper clamp of an EZ-S mechanical tester (Shimadzu). Measurements were performed in compression mode using a 10 N load cell, with a constant strain applied at 0.2 mm s^{-1}, and recording the force over time. Distilled water was used as a control.

Gel Modulus Measurement: Modulus was determined using both compression and indentation tests as previously described[9]. Briefly, compression testing was performed using

an EZ-S mechanical tester fitted with a 10 N load cell, with samples tested at a strain rate of 2 mm min^{-1}. The compression modulus (E_{Comp}) was calculated from the stress-stain curve, with three different samples used for testing and the average values reported. Indentation modulus (E_{Ind}) was also evaluated using an EZ-S mechanical tester but a flat stainless steel indenter (1 mm in diameter) with a 2 N load cell was used to indent the samples at a rate of 0.1 mm/min. Again, three different samples were tested at a minimum of four different locations per sample.

Diffusion Studies: Diffusion of solute into the gels was measured similarly to previously described method[8, 10]. Three cylindrical hydrogels (n=3) of 2 cm x 0.35 cm diameter were immersed in PBS containing fluorescently labeled bovine serum albumin (FITC-BSA, 250 µg/ml, Sigma) and maintained at constant temperature of 37 ºC in a shaking water bath. Protein uptake was determined by sampling the solution and measuring the loss of protein over time until it reached equilibrium using a micro-plate reader (Fluostar Omega, BMG Labtech). Concentrations of BSA were calculated from a standard curve. Diffusion coefficients of FITC-BSA in the gels were calculated using a nonlinear regression method and modelled using the finite element method (COMSOL 4.2)[10, 25, 26].

Scanning Electron Microscopy (SEM): For surface porosity studies, samples were submersed in hNSC culture media for 24 hr, freeze dried overnight using a Christ Alpha 2-4 LD Freeze Dryer, then coated with gold (20 nm) using an Edwards sputter coater, and kept desiccated until analysed.   SEM was performed using a JSM-7500FA LV Scanning Electron Microscope. For studies of internal porosity with and without cells, samples were fixed with 3.7% paraformaldehyde (PFA, Fluka) for 30 min, immersed in liquid nitrogen for 60 seconds, and then freeze-fractured using a cold razor blade. The fractured samples were immediately observed on the JSM-6490 LV Scanning Electron Microscope.

Live/Dead hNSC Analysis: Calcein AM (5 µg/ml, Life Technologies) and propidium iodides (PI, 5 µg/ml, Life technologies) were used to identify live and dead cells respectively,

according to the manufacturer's instructions. Briefly, hNSC-laden constructs were incubated with Calcein AM at 37 $^\circ$C for 10 min, followed by a media change, incubation with PI for 1 min, and a further media change. A confocal microscope (Leica TSC SP5 II) was used for image acquisition, with images from a minimum of five optical planes *per* construct merged (to capture the maximal projection of whole cell aggregates) for analysis using Fiji (Image J) software. Three independent samples were evaluated for each gel composition. Depth coding of cells shown in Supplementary Fig. 2 was performed using the 3D Projection Tool in Leica Application Suite X (LAS X) software (Leica).

hNSC Proliferation Analysis. PrestoBlue™ cell viability reagent was used for hNSC proliferation studies, according to the manufacturer's instructions. Briefly, at each time point measured, three hNSC-laden constructs were incubated with the reagent in culture medium for 1 hr at 37 $^\circ$C. Following incubation, for each sample, supernatant (100 µl) was transferred to a well of a 96-well plate and screened by a microplate reader (POLARstar Omega) to read fluorescence intensity. After processing, constructs were rinsed in culture medium and returned to culture, with the process repeated for each time point until the study was completed.

Immunocytochemistry: Samples were fixed with 3.7 % PFA solution in PBS at RT for 30 min, rinsed in PBS, and then blocked and permeabilized overnight at 37 $^\circ$C with 5% (v/v) donkey serum in PBS containing 0.3% (v/v) Triton X-100 (Sigma). Samples were subsequently incubated with fluorescence conjugated antibodies GFAP (mouse, 1:100; Cell signalling), SOX2 (rabbit, 1:100; Cell signalling), vimentin (rabbit, 1:200; Cell signalling), OLIGO2 (mouse, 1:100; Millipore), KI67 (mouse, 1:200; Invitrogen), TUJ1 (mouse, 1:100; Abcam) and nestin (mouse, 1:100; Invitrogen), or unconjugated primary antibodies synaptophysin (rabbit, 1:200; Millipore), GABA (rabbit, 1:200; Sigma) and GAD (rabbit, 1:500; Millipore) at 4°C overnight. On the second day, samples were rinsed with 0.1% Triton X-100 in PBS three times, and samples with unconjugated primary antibody were incubated

13

with Alexa Fluor tagged secondary antibody (1:1000; Invitrogen) for 1 hr at 37 °C. Nuclei were visualised with 4',6-diamidino-2-phenylindole (DAPI, 10 µg/ml) at RT for 10 min and antifade reagent (Invitrogen) was employed to preserve fluorescence signal. Samples were mounted onto glass coverslips using Aquamount (ThermoScientific) and imaged on a confocal microscope (Leica TSC SP5 II). Images were collected and analysed using Leica Application Suite AF (LAS AF) software (Leica).

Real Time Quantitative PCR (RT-qPCR): Gel-encapsulated cells were extracted for subsequent RNA isolation by treatment with disodium ethylenediamine tetraacetate (EDTA; 0.05 M) for 10 min to dissolve the gel[27]. After treatment, samples were centrifuged at 600 g for 5 min to collect the cells. Total RNA was then isolated using Trizol reagent (Invitrogen) and the quantity and purity of RNA was assessed using a NanoDrop™ 2000c Spectrophotometer (Thermo Scientific). RNA was transcribed to cDNA with random primers and RT-qPCR was performed using a Gotaq 2-step RT-qPCR Kit (Promega) on a Bio-Rad CFX real time instrument. The data were analyzed using the delta-delta Ct method. For primer sequences, see Table S1, Supporting Information.

Calcium Imaging: For calcium imaging, samples were loaded with Fluo-4 (23917; 2 µM; Life Technologies) in fresh culture medium, incubated for 30 min at 37 °C, and washed with Tyrode's solution (5 mM KCl, 129mM NaCl, 2mM CaCl2, 1mM MgCl2, 30mM D-Glucose and 25 mM HEPES, Ph 7.4)[28]. Samples were mounted on coverslips and imaging was performed at RT on a confocal microscope (Leica TSC SP5 II). LAS AF Lite software (Leica) was used to collect and quantify time-lapse excitation ratio images. GABA(A) receptor antagonist bicuculline (50 µM; Sigma) was added into Tyrode's solution for 3 min to induce intracellular calcium. Depth coding of cells was performed using the 3D Projection Tool in LAS AF software (Leica).

Statistical Analyses: Statistical analyses were performed in OriginPro 2015 (Version b9.2.272) using one-way analysis of variance (ANOVA) with Bonferroni multiple

comparison *post hoc* test or two-way ANOVA with Bonferroni *post hoc* test. Homogeneity of variance tests were performed to confirm statistical assumptions were met for ANOVA. Statistical significance was set at $P < 0.05$.

Acknowledgments

References

[1] S. V. Murphy, A. Atala, *Nat Biotechnol* **2014**, *32*, 773.

[2] P. R. Sivashankari, M. Prabaharan, *International journal of biological macromolecules* **2016**.

[3] A. L. Rutz, K. E. Hyland, A. E. Jakus, W. R. Burghardt, R. N. Shah, *Adv Mater* **2015**, *27*, 1607.

[4] T. Billiet, E. Gevaert, T. De Schryver, M. Cornelissen, P. Dubruel, *Biomaterials* **2014**, *35*, 49.

[5] O. Jeon, E. Alsberg, *Adv Funct Mater* **2013**, *23*, 4765.

[6] F. Pati, J. Jang, D. H. Ha, S. Won Kim, J. W. Rhie, J. H. Shim, D. H. Kim, D. W. Cho, *Nat Commun* **2014**, *5*, 3935.

[7] L. Ouyang, R. Yao, S. Mao, X. Chen, J. Na, W. Sun, *Biofabrication* **2015**, *7*, 044101.

[8] R. Lozano, L. Stevens, B. C. Thompson, K. J. Gilmore, R. Gorkin, 3rd, E. M. Stewart, M. in het Panhuis, M. Romero-Ortega, G. G. Wallace, *Biomaterials* **2015**, *67*, 264.

[9] J. H. Y. Chung, S. Naficy, Z. Yue, R. Kapsa, A. Quigley, S. E. Moulton, G. G. Wallace, *Biomaterials Science* **2013**, *1*, 763.

[10] R. H. Li, D. H. Altreuter, F. T. Gentile, *Biotechnol Bioeng* **1996**, *50*, 365.

[11] M. A. Green, L. E. Bilston, R. Sinkus, *NMR Biomed* **2008**, *21*, 755.

[12] S. A. Kruse, G. H. Rose, K. J. Glaser, A. Manduca, J. P. Felmlee, C. R. Jack, Jr., R. L. Ehman, *Neuroimage* **2008**, *39*, 231.

[13] Z. S. Xu, R. J. Lee, S. S. Chu, A. Yao, M. K. Paun, S. P. Murphy, P. D. Mourad, *J Ultrasound Med* **2013**, *32*, 485.

[14] Z. Taylor, K. Miller, *J Biomech* **2004**, *37*, 1263.

[15] S. R. Shin, H. Bae, J. M. Cha, J. Y. Mun, Y. C. Chen, H. Tekin, H. Shin, S. Farshchi, M. R. Dokmeci, S. Tang, A. Khademhosseini, *ACS Nano* **2012**, *6*, 362.

[16] K. Y. Lee, D. J. Mooney, *Prog Polym Sci* **2012**, *37*, 106.

[17] L. Upadhyaya, J. Singh, V. Agarwal, R. P. Tewari, *Carbohydrate Polymers* **2013**, *91*, 452.

[18] V. Patrulea, V. Ostafe, G. Borchard, O. Jordan, *European journal of pharmaceutics and biopharmaceutics : official journal of Arbeitsgemeinschaft fur Pharmazeutische Verfahrenstechnik e.V* **2015**, *97*, 417.

[19] D. E. Weinstein, M. L. Shelanski, R. K. Liem, *J Cell Biol* **1991**, *112*, 1205.

[20] F. W. Pfrieger, B. A. Barres, *Science* **1997**, *277*, 1684.

[21] E. M. Ullian, S. K. Sapperstein, K. S. Christopherson, B. A. Barres, *Science* **2001**, *291*, 657.

[22] J. W. Cave, M. Wang, H. Baker, *Front Neurosci* **2014**, *8*, 16.

[23] M. Ahearne, Y. Yang, K. K. Liu, "Mechanical characterisation of hydrogels for tissue engineering Applications", in *Topics in Tissue Engineering*, N. Ashammakhi, R. Reis, and F. chiellini, Eds., Ahearne: Publications 2008, p. 1.[24] D. L. Cohen, W. Lo, A. Tsavaris, D. Peng, H. Lipson, L. J. Bonassar, *Tissue Eng Part C Methods* **2011**, *17*, 239.

[25] P. C. Carman, R. A. W. Haul, *Proceedings of the Royal Society of London. Series A, Mathematical and Physical Sciences* **1954**, *222*, 109.

[26] J. Crank, "*The Mathematics of Diffusion"*, Second edition, Oxford University Press, New York, 1975.

[27] B.-h. Chueh, Y. Zheng, Y.-s. Torisawa, A. Y. Hsiao, C. Ge, S. Hsiong, N. Huebsch, R. Franceschi, D. J. Mooney, S. Takayama, *Biomedical microdevices* **2010**, *12*, 145.

[28] M. W. Radomski, R. M. Palmer, S. Moncada, *Proc Natl Acad Sci U S A* **1990**, *87*, 10043.
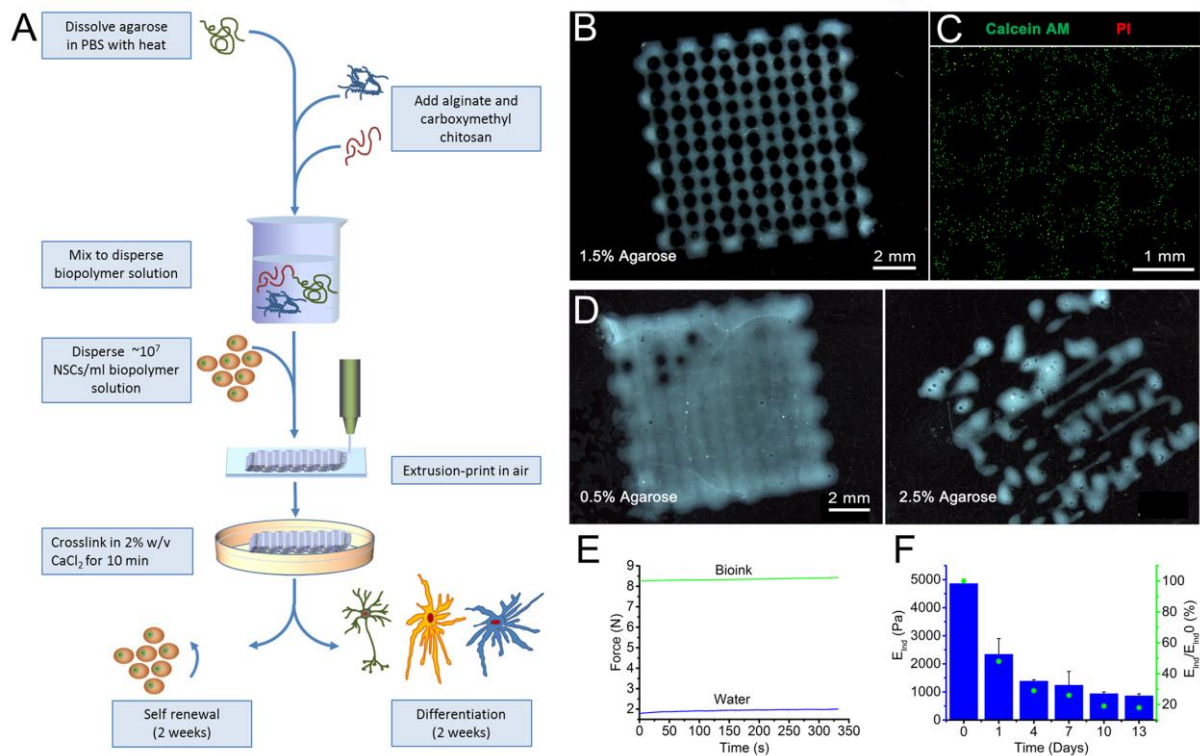
Figure 1. Generation of 3D nMTCs with optimal hNSC-laden Al-CMC-Ag bioink. A) Schematic illustrating the major stages of the method for direct-write printing hNSCs with bioink for 3D culture and differentiation. B) Printed gel scaffold comprising optimal 5% w/v Al, 5% w/v CMC and 1.5% w/v Ag. C) Live (Calcein AM) and dead (propidium iodide; PI) hNSC staining within optimal printed gel scaffold. D) Poorly defined scaffold structures comprising 0.5% and 2.5% w/v Ag. E) Consistency/homogeneity of optimal bioink (green line) demonstrated by extrusion force required for printing. Water control (blue line) employed for comparison. F) Indentation modulus (EInd; blue bars) of optimal gel over time (mean ± S.D.; n = 3) and % modulus (green dots) remaining at a specified time point relative to the initial modulus at day 0 (EInd0).
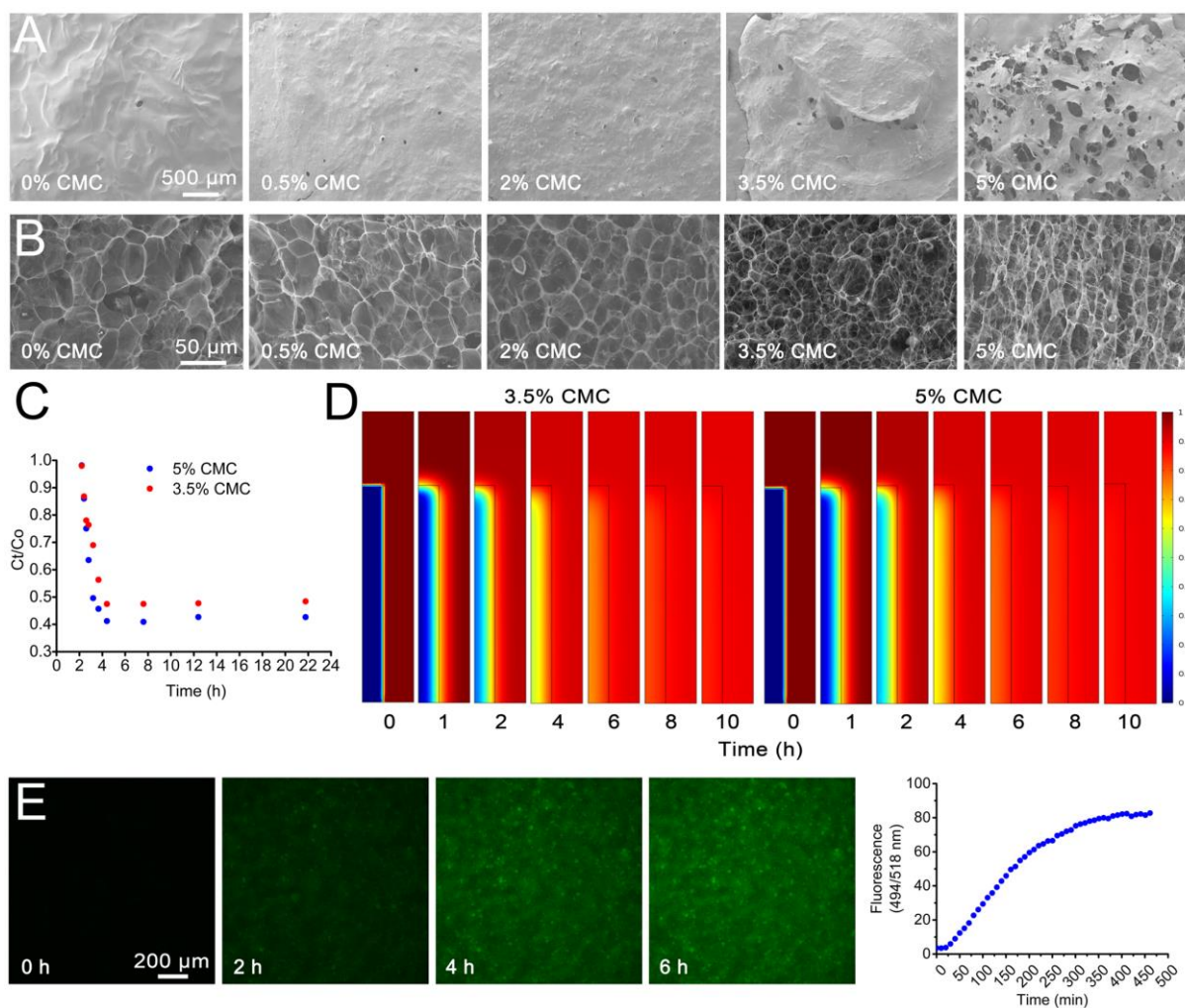
18

Figure 2. Characterization of porosity and permeability of gels. A) SEM showing surface porosity of gels with different concentrations of CMC. B) SEM showing internal porosity of gels with different concentrations of CMC. C) Uptake by diffusion of FITC-BSA from immersion solution into 5% and 3.5% w/v CMC gels. Diffusion of BSA from solution into submerged gels is indicated by decreasing measures of fluorescence in solution (data for a specific time point normalized against data for initial time point; C_t/C_0). D) Finite element model of BSA diffusion into 5% and 3.5% w/v CMC gels (COMSOL Multiphysics 5.0: 2D axisymmetric; 2 domains: gel (small/inset rectangle) and solution (large/enclosing rectangle)). E) Assessment by confocal microscopy of FITC-BSA diffusion through optimal 5% w/v CMC gel. Photomicrographs and quantitative data show increasing fluorescence intensity at a single optical plane and distal from the point of delivery (see also Figure S1 and Video S2, Supporting Information), supporting diffusion throughout the gel.
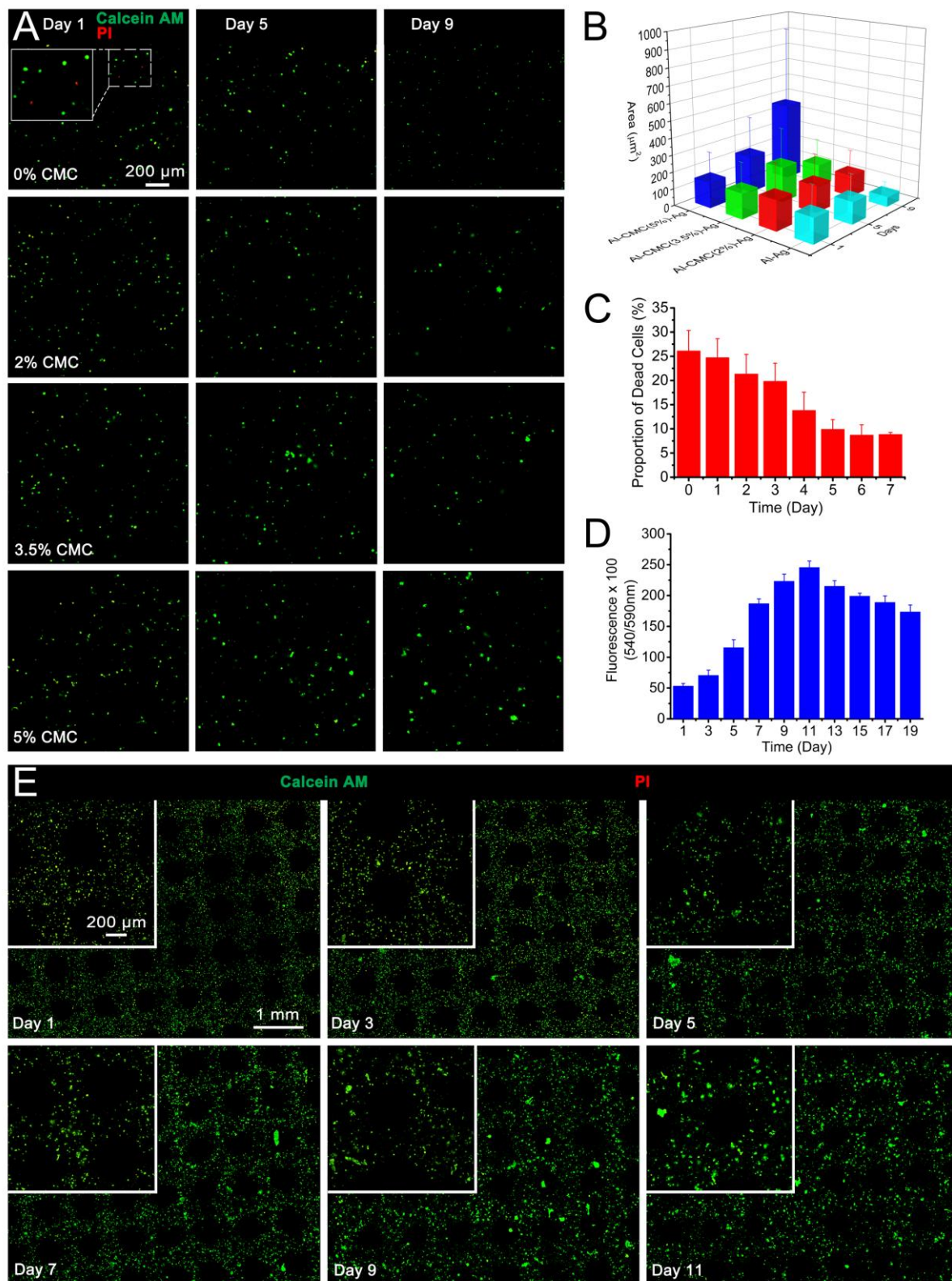
19

Figure 3. Survival and proliferation of printed hNSCs. A) Live (Calcein AM) and dead (propidium iodide; PI) hNSC staining at specific time points following direct-printing in gels with different concentrations of CMC. hNSCs are visible as single cells and aggregates of cells. B) Comparative assessment of viable hNSC content of constructs depicted in (A) including single cells and aggregates of cells by measuring the area of Calcein AM staining within constructs. Mean ± S.D.; n = 3. Two-way ANOVA with Bonferroni multiple comparison post hoc test. *P < 0.05 (3.5% w/v CMC day 5, vs Al-Ag day 9); **P < 0.01 (5%

20

w/v CMC day 5, vs Al-Ag day 9); ***P < 0.0001 (5% w/v CMC day 9 vs all comparisons). C) Time course of dead hNSC content of optimal 5% w/v CMC gel from day 0 to day 7 after printing (mean ± S.D.; n = 3). One-way ANOVA with Bonferroni post hoc test. * P < 0.001 (day 4 vs day 0). D) Time course of live (PrestoBlue™ cell viability indicator) hNSC content of optimal 5% w/v CMC gel from day 1 to day 19 after printing (mean ± S.D.; n = 3). One-way ANOVA with Bonferroni post hoc test. * P < 0.0001 (day 5 vs day 1). E) Printed hNSCs within the optimal gel construct showing grid/scaffold structure at specific time points. hNSCs are initially visible as single cells immediately following printing (day 1), with aggregates of cells increasingly apparent over time (day 3 – day 11). See also Figure S2, Supporting Information.
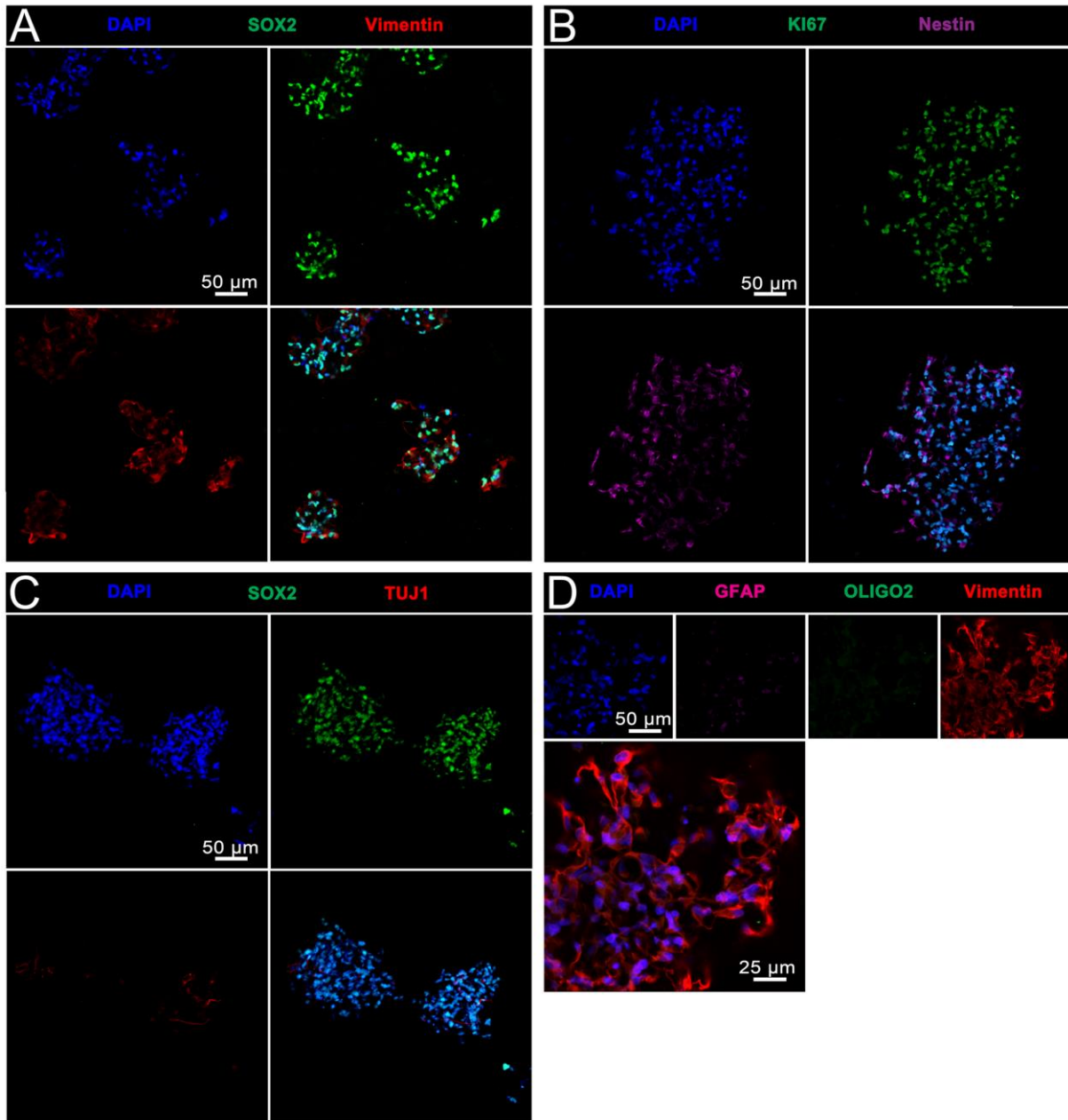
Figure 4. Immunophenotyping of hNSCs encapsulated within an optimal gel construct 3 weeks after printing. A) hNSCs stained with DAPI colocalized with SOX2, and expressed vimentin. B) Cells also expressed nuclear proliferation marker KI67 and hNSC marker nestin. C) hNSCs expressed negligible levels of differentiated neuron marker TUJ1. D) hNSCs expressed negligible levels of differentiated astrocyte and oligodendroglial lineage markers GFAP and OLIGO2 respectively.
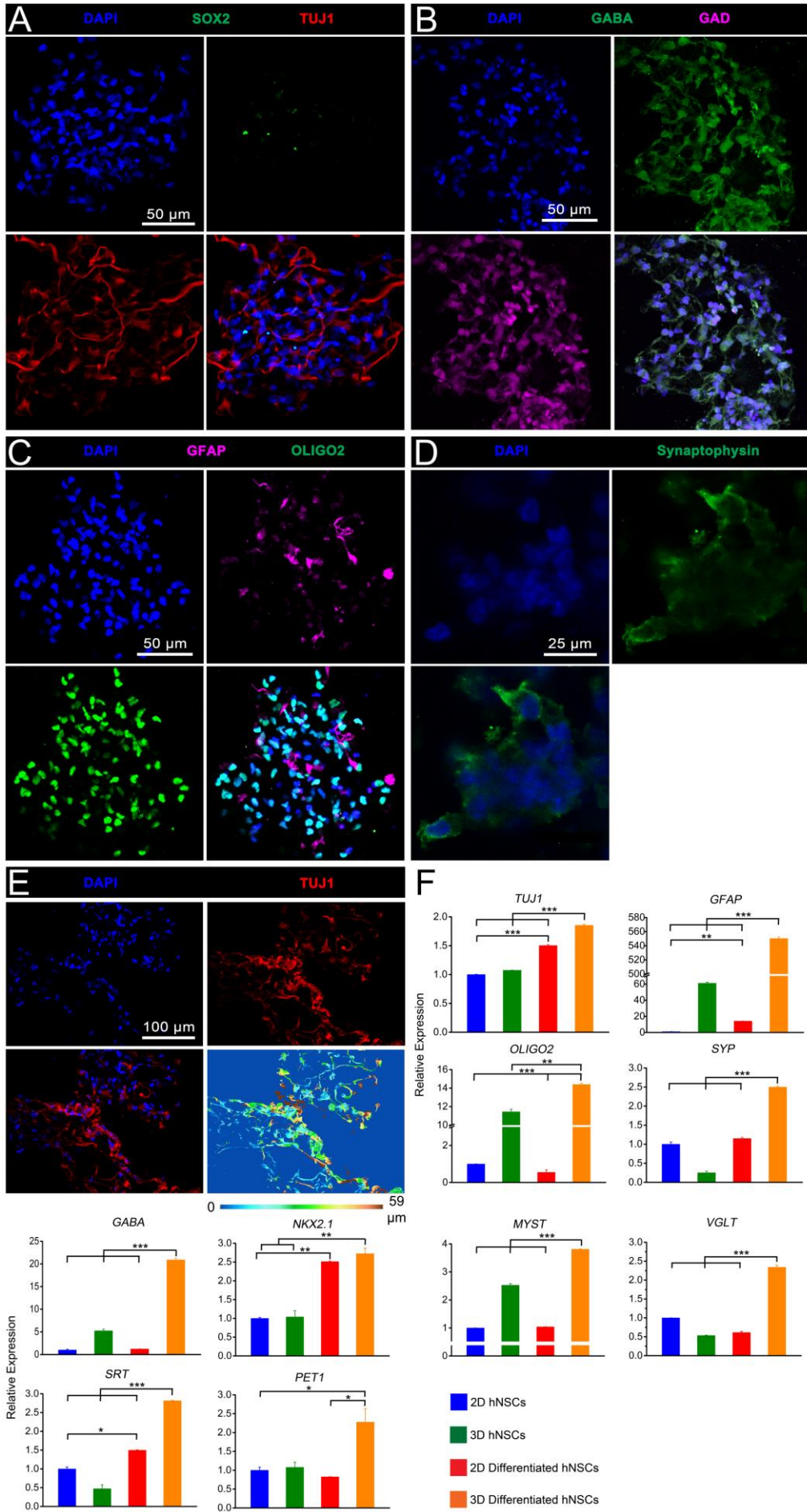
Figure 5. Immunophenotyping and gene expression of differentiated hNSCs encapsulated within an optimal gel construct. A) Cells (24 days post-printing, including 14 days differentiation) stained with DAPI and expressed neuronal marker TUJ1 with negligible levels of hNSC marker SOX2 (see also Supplementary Video 3). B) Neurons expressing GABAergic neuron markers GABA and GAD. C) Gliogenesis within neural constructs supported by astrocyte and oligodendroglial lineage markers GFAP and OLIGO2 respectively. D) Synaptogenesis within neural constructs illustrated by presynaptic protein synaptophysin. E) Cells (31 days post-printing, including 21 days differentiation) stained with DAPI and expressed TUJ1, with cell clusters interconnected by neurites. The lower right panel shows depth coding of cells along the Z-axis (0 − 59 μm). F) Comparative gene expression between conventional 2D and printed 3D hNSC culture (3 weeks) and differentiation (5 days initial hNSC culture followed by 16 days of differentiation). Relative gene expression represents data normalized to β-actin and expressed relative to 2D hNSCs. Mean ± S.D.; n = 3. One-way ANOVA with Bonferroni post hoc test. *P < 0.05; **P < 0.01; ***P < 0.001.
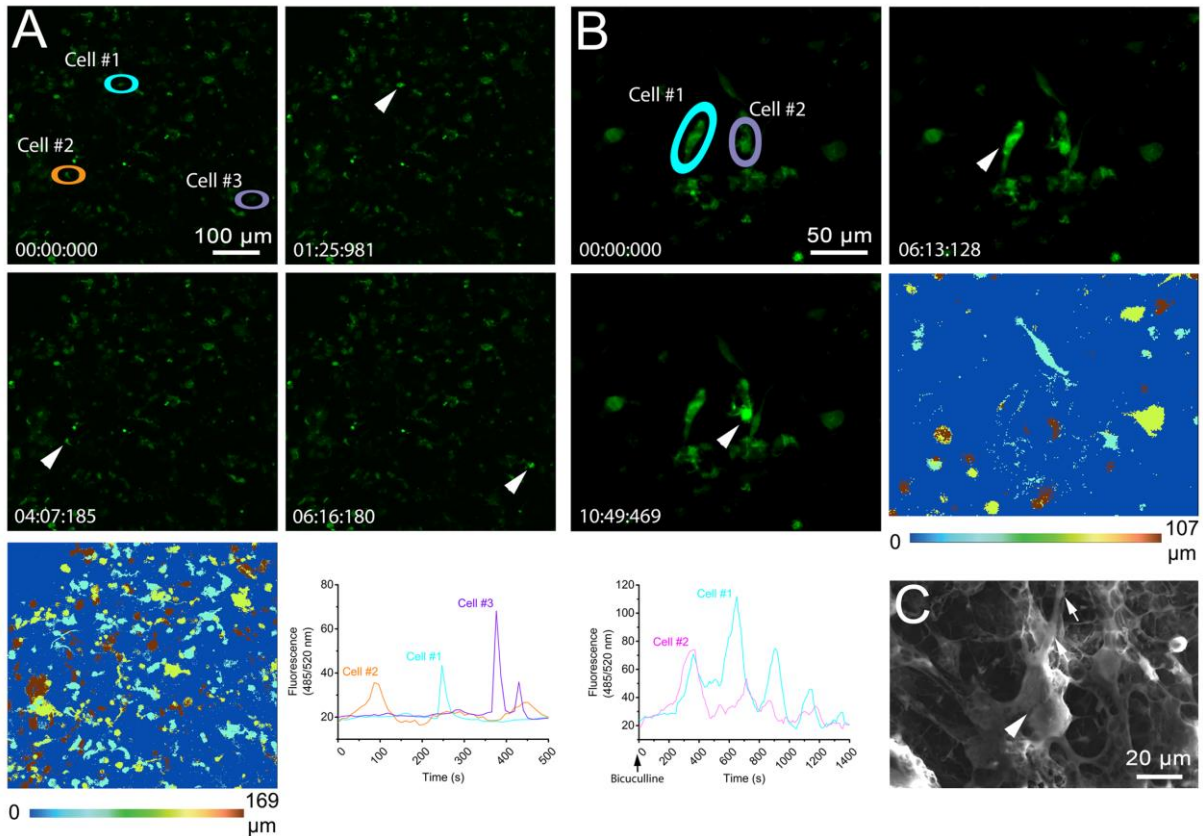
Figure 6. Functional maturation of in situ differentiated hNSCs in an optimal gel construct. A) Time course of live calcium imaging of neurons within a 3D construct, with the lower left panel showing depth coding of cells along the Z-axis (0 − 169 μm; i.e. different colors represent different planes along the Z-axis), and average measurements of spontaneous activity for cells 1-3 of photomicrographs demonstrated by the corresponding plot. Arrowheads indicate active cells (see also Video S4, Supporting Information). B) Time course of live calcium imaging of neurons within a 3D construct, with the middle right panel showing depth coding of cells along the Z-axis (0 − 107 μm), and average measurements of bicuculline-induced calcium response for cells 1-2 of photomicrographs demonstrated by the corresponding plot. Arrowheads indicate active cells (see also Video S5, Supporting Information). C) SEM image showing a neuron inside a porous 3D construct, with an arrowhead and arrow indicating a rounded cell soma and extending neurite respectively.